Available online at www.sciencedirect.com
SCIENCE DIRECT
ELSEVIER
International Journal of Machine Tools & Manufacture 46 (2006) 1879–1891
INTERNATIONAL JOURNAL OF MACHINE TOOLS & MANUFACTURE DESIGN, RESEARCH AND APPLICATION
www.elsevier.com/locate/ijmactool

Laser-assisted machining of Inconel 718 with an economic analysis

Mark Anderson, Rahul Patwa, Yung C. Shin*

Center for Laser-based Manufacturing, School of Mechanical Engineering, Purdue University, West Lafayette, IN 47907, USA

Received 21 July 2005; received in revised form 28 October 2005; accepted 3 November 2005
Available online 18 January 2006

Abstract

Superalloys have high strengths at elevated temperatures, which make them attractive toward various applications and also make these materials difficult to machine at room temperature due to excessive tool wear and poor surface finish. Laser-assisted machining (LAM) offers the ability to machine superalloys more efficiently and economically by providing the local heating of the workpiece prior to material removal by a single point cutting tool.

An existing transient, three-dimensional heat transfer model is modified for modeling LAM of Inconel 718. Suitable coating conditions are determined for increasing the laser absorptivity in metals and an approximate absorptivity value is determined. The thermal model is validated in axial and circumferential directions by temperature measurement using an infrared camera.

The machinability of Inconel 718 under varying conditions is evaluated by examining tool wear, forces, surface roughness, and specific cutting energy. With increasing material removal temperature from room temperature to 620 °C, the benefit of LAM is demonstrated by a 25% decrease in specific cutting energy, a 2–3-fold improvement in surface roughness and a 200–300% increase in ceramic tool life over conventional machining. Moreover, an economic analysis shows significant benefits of LAM of Inconel 718 over conventional machining with carbide and ceramic inserts.

Keywords: Laser-assisted machining; Inconel 718; Superalloys; Machinability; Economic analysis

1. Introduction

Laser-assisted processing of material is one of the emerging fields in advanced manufacturing. The advantages that make the lasers increasingly attractive in industrial production include coherence, focusability, very high power intensity, power shaping capability, and ease of automation with in-process sensing [1]. It also offers the potential to realize innovative design with high flexibility, a high processing speed, and good quality in many manufacturing processes. The capital investment may be higher, but this is offset by the benefits gained in many applications.

Superalloys, such as nickel, iron-nickel, and cobalt-base alloys, have high strengths at elevated temperatures, show resistance to chemical degradation, and have high wear resistance. Inconel 718 is nickel-base superalloy, which is used in the field of gas turbine components, cryogenic storage tanks, jet engines, pump bodies and parts, rocket motors and thrust reversers, nuclear fuel element spacers, hot extrusion tooling, high strength bolting, and down hole shafting. The same properties that make superalloys attractive toward various applications also make these materials difficult to machine at room temperature due to excessive tool wear and poor surface finish. The associated manufacturing cost is high because of low material removal rates and rapid tool wear. In order to reduce overall machining costs, laser-assisted machining (LAM) is investigated for machining of Inconel 718.

Inconel 718 is a solid solution hardened or precipitation hardened alloy with an FCC structure. The composition is such that many different phases and precipitates readily form, varying in size, distribution, and location [2]. It receives much of its strength from small γ' and γ'' precipitates that are high in Ni and Al or Ti (typically: Ni_3Al/Ti). The yield strength of Inconel 718 decreases drastically above 650 °C until approximately 950 °C.

*Corresponding author. Tel.: +1 765 494 9775; fax: +1 765 494 0539.
E-mail address: shin@ecn.purdue.edu (Y.C. Shin).

0890-6955/$ - see front matter © 2005 Elsevier Ltd. All rights reserved.
doi:10.1016/j.ijmachtools.2005.11.005

LAM of metals uses a high power laser to provide the local heating of the workpiece prior to material removal by a single point cutting tool. The benefits of heating Inconel 718 prior to the material removal with a conventional cutting tool have been demonstrated by Rajagopal et al. [3], Novak and co-workers [4,5], and Leshock et al. [6]. These exploratory investigations demonstrated that surface roughness improvements, a decrease in specific cutting energy, and an increase in tool life as a result of thermally assisted machining of Inconel 718.

The concept of facilitating material removal during machining by locally heating materials has been around for many years. In the late 1970s, lasers emerged as a viable heat source, capable of producing intense heat in a very precise region. In 1978, Bass and co-workers showed the feasibility of "hot spot" laser machining using a 1400 W CO_2 laser to assist machining in stainless steels and Udimet 700. No modeling of the process was performed at this time, providing little insight into temperatures achieved during the process, but it was observed that coordination between the cutting speed and laser heating must be optimized, and that there are large inefficiencies in heating the metal as a result of the reflectivity of the workpieces. Later, Jau et al. [7] predicted temperatures in the shear area according to the Cline and Anthony [8] model of laser heating, and assumed an average temperature rise due to the workpiece plastic deformation to predict overall temperature rises within the shear zone. They estimated that 7 kW of laser power is necessary to achieve 100% improvement in the material removal rate in Inconel 718 using a silicate solution sprayed onto the workpiece to increase absorptivity.

Rajagopal et al. [3] experimented with a 14 kW CO_2 laser on titanium and Inconel 718, showing that beam location is important during LAM. Various coatings were studied, including India ink, silicon carbide, and potassium silicate with varying degrees of successful absorptivity enhancement. Due to inefficiencies associated with laser–metal interactions and the high initial cost of the laser, economic justification for LAM was not achieved and interest in LAM became diverted to other research.

Flom and co-workers [9] conducted research on LAM of Ti-6Al-4V and Inconel 718 using an Nd–YAG pulse laser, which has the advantage of providing higher absorptivity for metals due to its shorter wavelength. To overcome the intermittent energy problem he used two different techniques. Firstly, he used the laser as a primary heat source at a high pulse rate and observed a reduction in cutting forces by 49% and chip fragmentation during LAM of Inconel 718. For Ti-6Al-4V forces dropped by 30% in air and 60% with oxygen assist. Secondly, he used the laser to precondition the workpiece before machining and obtained 28% reduction in forces for Ti-6Al-4V. However, it lacked any detailed analysis and no improvements in tool wear and surface roughness were reported.

Recent plasma-enhanced machining (PEM) research shows the benefits that could be achieved in difficult-to-machine materials using a plasma arc as a heat source [4–6]. Although the amount of heat input to the workpiece in PEM is not limited by reflectivity problems of the metals, PEM causes extraneous heating to the bulk material, which may cause part distortion and adverse heat affected zones. On the other hand, LAM provides precise control of deposited energy and heated region, thereby avoiding any undesirable heating of the finished surface. Therefore, it is much more attractive from the view point of ensuring desired subsurface conditions of a machined part.

Even though previous researchers have shown the feasibility of LAM of metals, significant benefits in tool life and surface condition need to be demonstrated. In order to do this, governing root causes for the insufficient gain of LAM over conventional machining need to be separated out and minimized. The objectives for this study on LAM are to (i) apply a thermal model for LAM to accurately predict and characterize the thermal fields of Inconel 718 undergoing LAM, (ii) experimentally verify such predictions using surface temperature measurements for a wide range of operating parameters, (iii) utilize this validated model to discern the underlying physical phenomena, which include machinability, material removal mechanism, tool wear mechanism, and tool wear rate, and (iv) find optimized operating ranges of process parameters for LAM of Inconel 718.

2. Thermal model

A transient, three-dimensional thermo-mechanical model of a rotating workpiece undergoing laser heating and material removal was first developed by Rozzi et al. [10–12] for an opaque homogenous ceramic workpiece. The schematics of workpiece geometry with the complete heat transfer problem is shown in Fig. 1. Assuming isotropic thermal conductivity, the heat equation governing this phenomenon is given by

$$\underbrace{\rho\omega\frac{\partial h}{\partial \phi}+\rho V_z\frac{\partial h}{\partial z}}_{\text{advection}}+\underbrace{\rho\frac{\partial h}{\partial t}}_{\text{storage}} = \underbrace{\frac{1}{r}\frac{\partial}{\partial z}\left[rk\frac{\partial T}{\partial r}\right]+\frac{1}{r^2}\frac{\partial}{\partial \phi}\left[k\frac{\partial T}{\partial \phi}\right]+\frac{\partial}{\partial z}\left[k\frac{\partial T}{\partial z}\right]}_{\text{conduction}}+\underbrace{q'''}_{\text{generation}}, \tag{1}$$

where ρ is the density in kg/m^3, ω the rotational speed in rad/s, h the enthalpy in J/kg, k the thermal conductivity in W/mK, and r, ϕ, and z are cylindrical coordinates in m.

In the above equation, circumferential advection arises from the rotation of the workpiece and axial advection arises because the coordinates are fixed relative to the laser heating and/or machining. In order to account for the variation of specific heat with temperature, the numerical solution for the current heat transfer problem given in

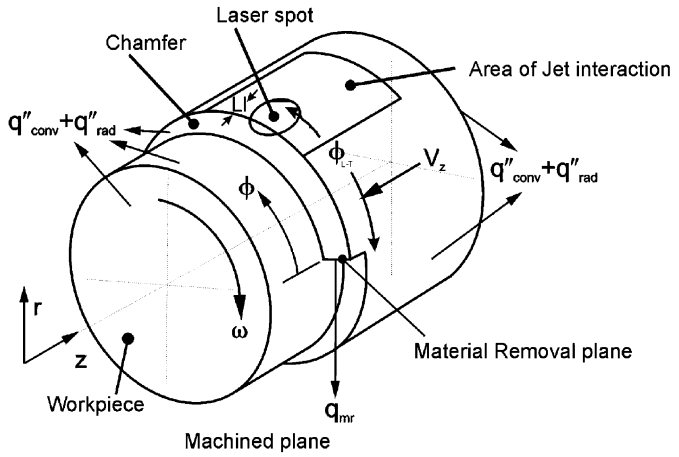

Fig. 1. Model geometry for the laser-assisted machining of a cylindrical workpiece [10].

Eq. (1) can be written as [13]

$$\rho\omega\frac{\partial(c_pT)}{\partial\phi}+\rho V_z\frac{\partial(c_pT)}{\partial z}+\rho\frac{\partial(c_pT)}{\partial t}=\frac{1}{r}\frac{\partial}{\partial z}\left[rk\frac{\partial T}{\partial r}\right]+\frac{1}{r^2}\frac{\partial}{\partial\phi}\left[k\frac{\partial T}{\partial\phi}\right]+\frac{\partial}{\partial z}\left[k\frac{\partial T}{\partial z}\right]+q'''+\rho\omega\frac{\partial(c_pT^*-h^*)}{\partial\phi}+\rho V_z\frac{\partial(c_pT^*-h^*)}{\partial z}+\rho\frac{\partial(c_pT^*-h^*)}{\partial t}, \quad (2)$$

where T^* and h^* are the values of T and h gained from the previous iteration and used to solve for T in current iteration. When convergence is achieved, T^* and h^* are equal to T and h, respectively.

In order to solve the governing Eq. (2), it is needed to define proper boundary conditions. The detailed descriptions of the boundary conditions are skipped here for brevity and referred to Rozzi et al. [10] and Rebro et al. [14]. The complete computational domain is defined by boundary conditions that involve mixed convection, emitted radiation, and absorbed laser radiation. Rozzi et al. [11] provide the further details for the thermal model regarding geometric approximations, free and forced convection correlations, air-jet correlations, etc.

After formulating the above equations, a numerical solution of the above problem was obtained. A numerical code based on the finite volume method was used to discretize the given equations [11]. The workpiece was divided into a set of predefined control volumes $52\times42\times72$ (Φ, r, z) and size of mesh under the laser was equal to 0.35 mm for z, 0.06 mm for r, and 0.014 rad for ϕ. By doubling the control volumes in the circumferential direction it was observed that the temperature fields are independent of further decrease in grid size. Finer grids under the laser and near the material removal plane are possible, where temperature and their gradients are highest and of most interest to LAM, since the coordinate system is fixed relative to the laser. This resulted in saving a lot of computational time. An implicit scheme was used to attain convergence, which prevented any unrealistic oscillations in the solution [11]. Calculations marched in time until machined length is reached. At each time step a global energy balance convergence criterion was computed. This criterion had to be satisfied for four consecutive iterations before proceeding to the next time step.

Figs. 2 and 3 show the thermal conductivity and specific heat, respectively, of Inconel 718 measured by various investigators. The spread in the data is relatively small,

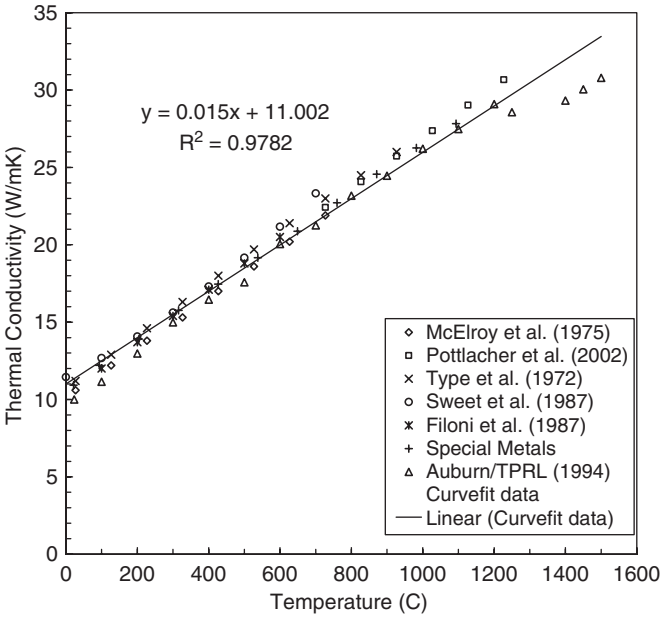

Fig. 2. Comparison of temperature-dependent thermal conductivity of Inconel 718.

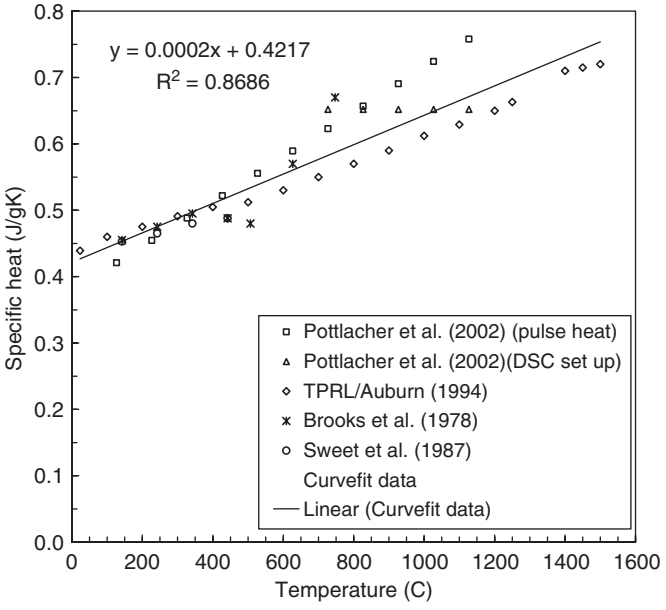

Fig. 3. Comparison of temperature-dependent specific heat of Inconel 718.

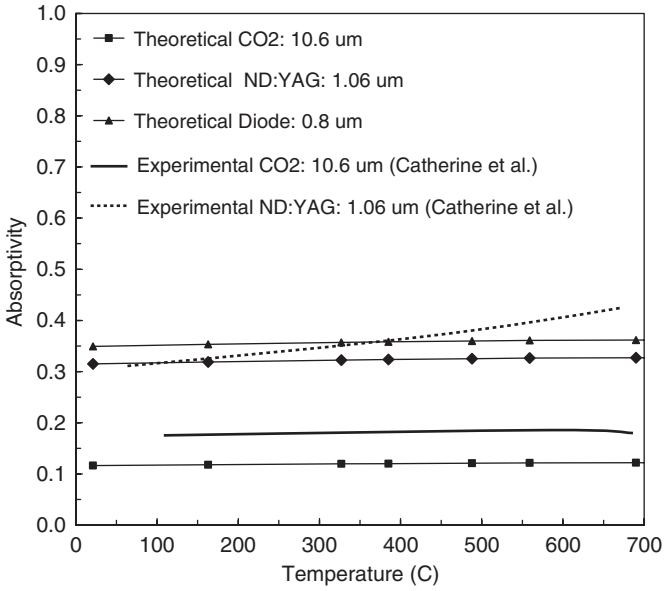

Fig. 4. Theoretical and experimental normal spectral absorptivity of Inconel 718 at different laser wavelengths.

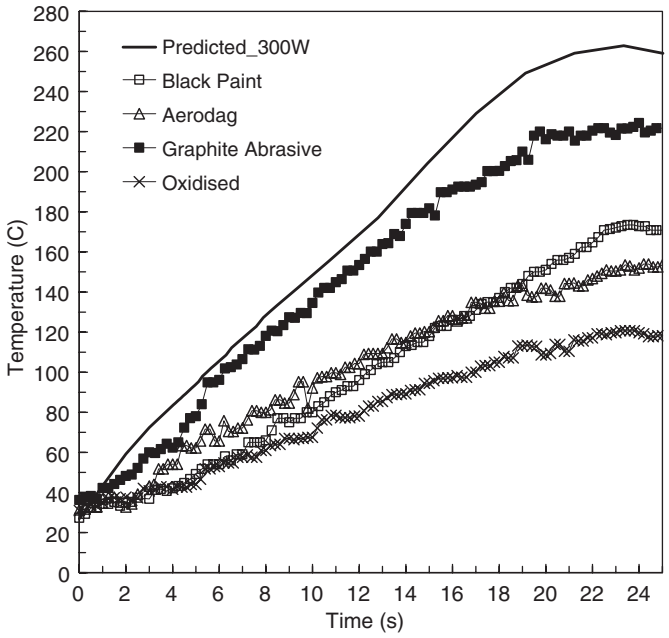

Fig. 5. Comparison of measured and predicted temperatures for power-300 W.

indicating that all of the data is precise and most likely accurate. Fig. 4 shows the experimental values of spectral absorptivity for Inconel 718 [15,16]. As can be seen, the absorptivity of Inconel 718 is very low for CO_2 lasers, while it is higher for shorter wavelength lasers, such as Nd:YAG and diode lasers.

3. Thermal model validation

3.1. Experimental arrangement

In order to overcome the low absorptivity of bare Inconel 718 to CO_2 laser, all parts are coated with graphite before laser heating is done. For five different coatings including three graphite coatings, viz., aerodag, aquadag, and graphite adhesive as well as oxide and black paint coating predicted using absorptivity of 1, and measured temperatures are compared over for different laser powers (100, 200, and 300 W). Fig. 5 shows the comparison for the complete heating cycle for 300 W power case. A common observation is that the measured temperature is always lower than the predicated temperature over the complete heating cycle irrespective of the coating type and condition. Moreover, the absolute difference in the temperature increases as the heating continues and is the largest at the highest temperature for all the cases. Yet, the percentage difference in the measured and predicted temperature remains fairly constant over the complete heating cycle. This indicates that approximate absorptivity values can be determined by adjusting α until they match for different coatings. Since the relative performance of graphite adhesive coating is far superior than the other tried coatings, it is therefore used for further experiments.

The emissivity of graphite binder was determined at the wavelength of different measuring instruments used. Table 1 lists the normal spectral emissivity values as determined at different wavelengths corresponding to different measuring instruments, viz., radiation pyrometer and long-wavelength infrared camera.

To verify the thermal model, two different non-contact temperature measuring devices have been utilized. The Williamson fiberview radiation pyrometer series 6000E is a non-contact measuring device monitoring temperature from one spot. It operates over a single waveband, which relies on a band pass filter that transmits radiation only around 2.2 μm wavelength to measure temperature in the working range of 250–650 °C. Calibration of the pyrometer was done prior to its first use using a blackbody calibration source and has also been calibrated regularly after moderate usage.

For heating-only tests, the pyrometer position is fixed along the circumferential plane close to the location of the cutting tool after the cutting tool was removed for these tests. It continuously measures the surface temperature from one spot while translating along with the laser. With a special fixture designed for holding the pyrometer probe, it could be moved 40–60° circumferentially from the laser. Fig. 6 shows the pyrometer fixture design for heating-only tests. The heating tests have been conducted using this setup with the intention of measuring temperature that would be generated in the vicinity of cutting tool.

A high performance ThermaCAM SC3000 infrared camera was later used to measure the surface temperature. Unlike the pyrometer, for measurements with the infrared camera, the workpiece is rotated in anticlockwise direction and the camera remains stationery while the laser

Table 1
Emissivity of graphite coating for different wavelengths

Instrument	Symbol	Wavelength range	Center wavelength	Spectral emissivity
Radiation pyrometer	ε_{pyro}	2.2	2.2	0.85
Long-wave infrared camera	ε_{ir}	8–9	8.5	0.88

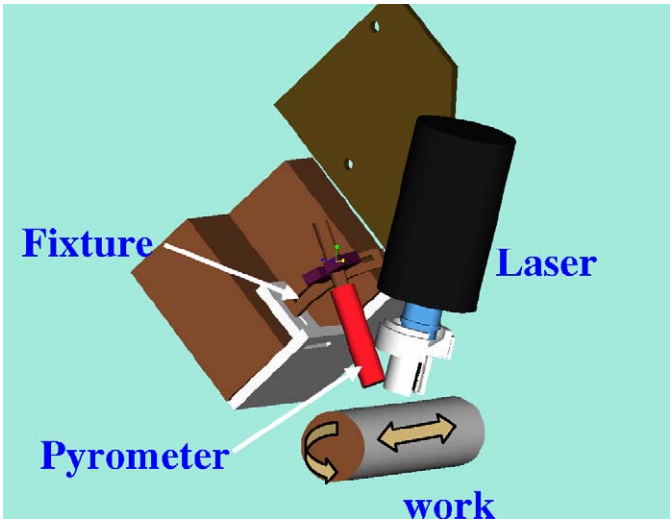

Fig. 6. Schematic illustration of in-process temperature measurement with a pyrometer.

translates. The measuring wavelength window of this device is 8–9 μm and the temperature sensing range set for the present case was 100–500 °C. The focal spot is perpendicular to the workpiece axis and 30° downstream from the laser spot, and remains stationery while the laser translates. The emissivity was set at 0.88, corresponding to the applied surface coating. The output is read directly from an attached PC data acquisition system using the software provided with the camera, which is very efficient in compensating for environmental and geometrical error factors, while calculating true surface temperature. The data were collected at 60 Hz and averaged for every five points. Since it can measure temperature with a large field of view, it is possible to measure the temperature at the same angular location throughout the heating process without moving the camera.

3.2. Experimental conditions

First, heating-only tests are conducted by translating the laser beam across the heating length while the workpiece is rotating and temperature is measured using either the radiation pyrometer or infrared system. No cutting tool is used during these tests. Table 2 shows the experimental test matrix for the heating-only tests conducted for thermal model validation. Two surface temperature measuring devices, viz., long-wavelength infrared camera and radiation pyrometer, have been employed. The purpose of these tests is to validate the thermal model (i) for the variation of laser power, (ii) in the circumferential direction, and (iii) for repeatability of coating conditions. The temperature measurement location of the infrared camera is shown in Fig. 7.

3.3. Validation results

Fig. 8 displays the measured and predicted temperature histories for 300 W (Test_Pre_IN_300). The temperature data below 100 °C is not shown in this plot as the temperature range was set at 100–500 °C in the infrared camera. At the beginning of the heating cycle, a smooth and relatively rapid increase in temperature matches very well with predicted temperature histories. For the case of 500 W power, the measured temperature was much lower than the predicted temperature during the complete heating cycle with increasing difference at higher temperatures. This discrepancy has been attributed to the lower absorptivity of metals to the laser at higher laser power. The coating gets off the surface by the high laser power energy at the preheating cycle and a portion of the bare metal surface is exposed, which results in lowering surface absorptivity.

Fig. 9 shows the variation of theoretical, predicted maximum temperature under the laser spot with increasing power. A sharp linear increase in temperature with power is evident from this plot, which can be used to explain the decreasing absorptivity and draw a bound for a safe maximum temperature. Since the coating cannot sustain itself on the surface for temperatures greater than approximately 1100 °C corresponding to 500 W case, it results in decreasing absorptivity and thus the measured temperatures.

Fig. 10 shows the comparison of measured and predicted maximum temperatures at a location axially aligned with and 40°, 55°, and 90° downstream from the laser center. The measurements have been performed using the infrared camera and the temperature data less than 100 °C are not shown as it was outside the temperature measurement range set in the infrared camera (100–500 °C). There is an excellent agreement between the measurements and prediction for 40° but it shows a larger discrepancy at higher angles of 55° and 90°, with measurements showing consistently lower temperatures than the predictions. One reason for such a deviation could be associated with modeling of the air-jet in the thermal model since the boundaries of air-jet exist till ±30 °C around the laser

Table 2
Experimental conditions for heating-only tests for Inconel 718

Case	Measuring device	P_l (W)	Angle (deg.)	Comparison parameter
Test_Pre_IN_200	IR camera	200	90	Power
Test_Pre_IN_300	IR camera	300	90	
Test_Pre_IN_400	IR camera	400	90	
Test_Pre_IN_500	IR camera	500	90	
Test_Pre_IN_300	IR camera	300	90	Circumferential temperature gradient
Test_Pre_IN_300	IR camera	300	55	
Test_Pre_IN_300	IR camera	300	40	
Test_Pre_IN_300	Pyrometer	300	45	Circumferential temperature gradient
Test_Pre_IN_300	Pyrometer	300	38	
Test_Pre_IN_400	IR camera	400	90	Experimental setup

$N = 200$ RPM; $D_l = 4.5$ mm; $f = 0.05$ mm/rev; $D_w = 40$ mm; $t_p = 4$ s; $\alpha = 0.8$; $\varepsilon_{ir} = 0.88$; $\varepsilon_{pyro} = 0.85$.
(1) Measured temperature corresponds to emissivity of Infrared camera set to 0.88 and pyrometer at 0.85.
(2) Rotation direction is counterclockwise. Length of travel is 11 mm (70 s).

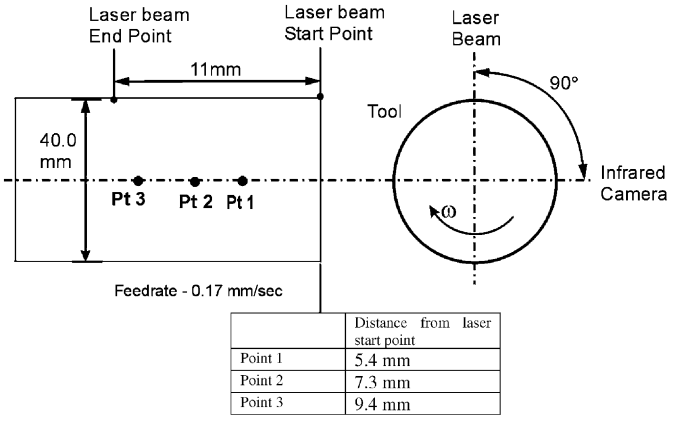

Fig. 7. Measurement locations for the infrared camera ($\lambda = 8-9\,\mu$m).

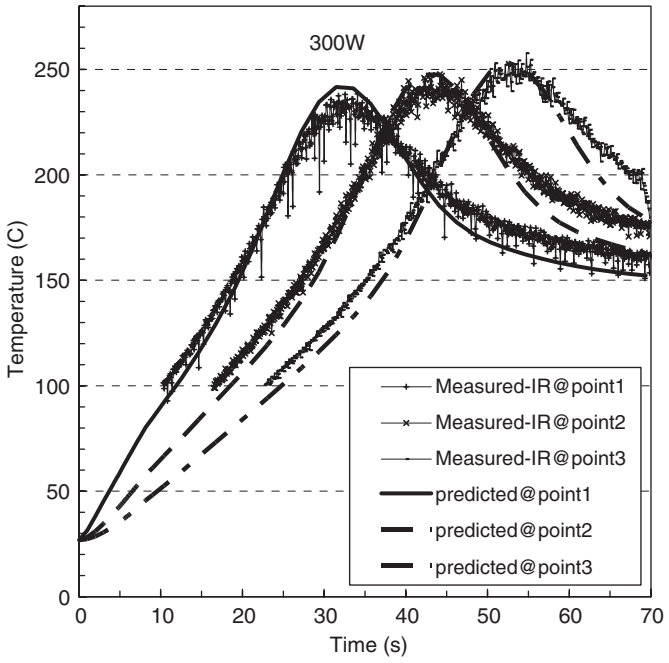

Fig. 8. Predicted and measured temperature history (300 W).

center. The agreement is good for the complete heating time of 70 s. Similarly, Fig. 11 shows the temperature comparison with the radiation pyrometer at circumferential locations 38° and 45° downstream from the laser center. For both locations, there is an excellent agreement between the measurements and prediction over the complete heating cycle. The temperature data less than 250 °C are not shown as it was outside the temperature measurement range of the radiation pyrometer (250–650 °C).

4. LAM experimental results

Proper control of coating conditions (thickness, uniformity, and surface adhesion) is an integral part of a good experimental setup. In order to test the repeatability of the experiment results, similar experimental conditions were repeated and measured temperatures were compared. The measurements in both cases overlap on the top of each other over the complete heating cycle, which shows that the setup has a high repeatability.

After validating the thermal model for the present application, LAM tests were designed and conducted. It is desired to achieve a material removal temperature of between 550 and 650 °C (T_{mr} is the material removal temperature generated by heating from the external source, i.e., laser and heat gun, and does not account for heat generated due to plastic deformation). This corresponds to the average temperature of the plane immediately before the beginning of the primary shear zone. The heat generated by plastic deformation in the primary shear zone will raise the local temperature by another 100–150 °C. At a temperature of approximately 750 °C Inconel experiences a sharp decrease in yield stress with increasing temperature. Therefore, Inconel 718 is much

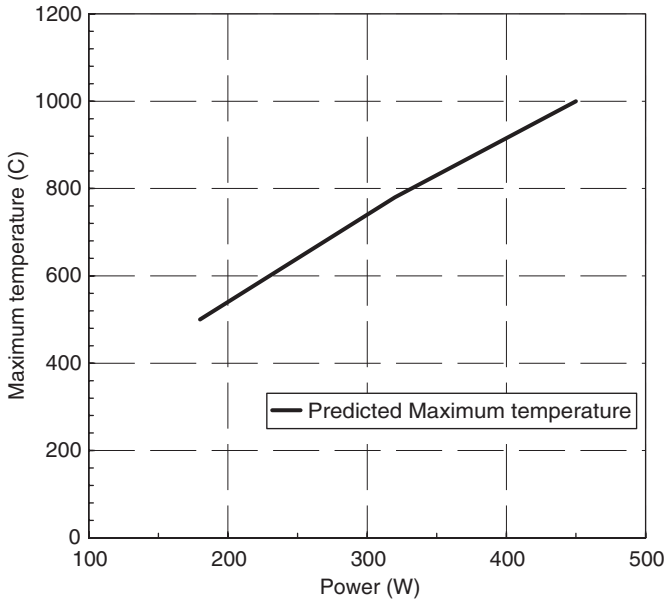

Fig. 9. Variation of maximum temperature under the laser spot with laser power.

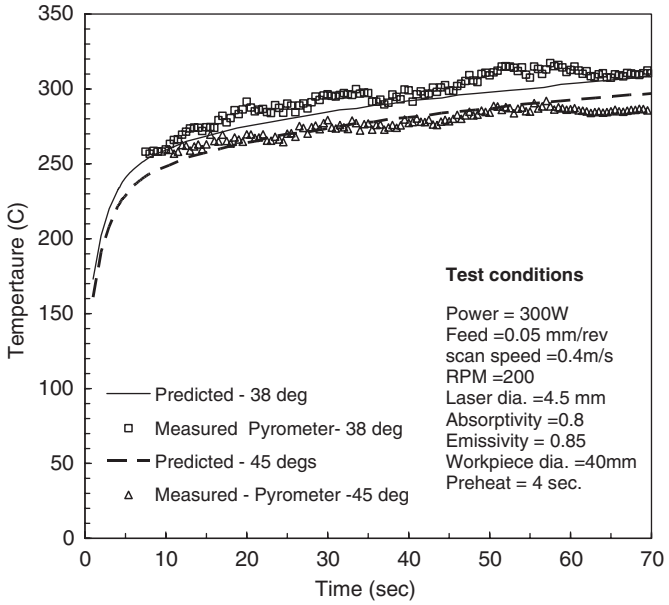

Fig. 11. Comparison of maximum predicted and measured temperature at different circumferential locations with the radiation pyrometer.

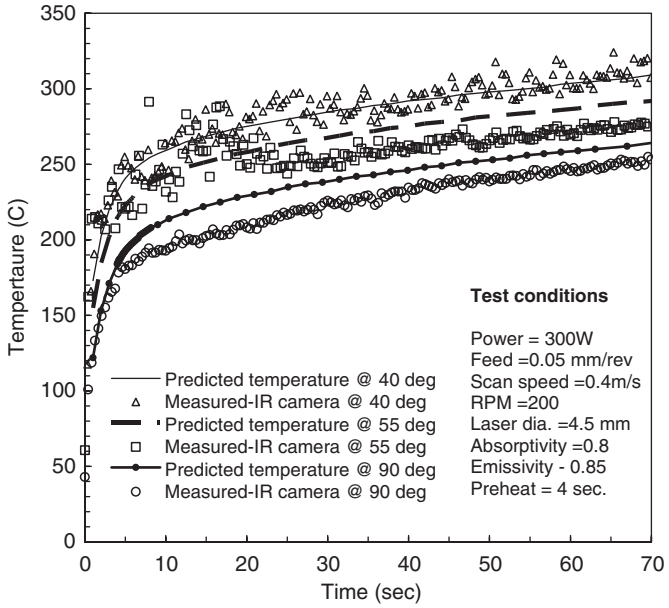

Fig. 10. Comparison of maximum predicted and measured temperature at different circumferential locations with infrared camera.

more machinable at 800 °C than at 600 °C. The benefit of thermally assisted machining of Inconel 718 has been very well demonstrated earlier by Novak and co-workers [4,5], Shin and Kim [17], Leshock et al. [6], and Rajagopal et al. [3]. Since it has been observed that the absorptivity value of 0.80 can be maintained only up to a maximum surface temperature of 1100 °C, achieving the desired material removal temperature is limited not only by the maximum laser power but also by the maximum allowable surface temperature. In addition, the material removal temperature is restricted by the current LAM setup that does not allow shorter circumferential angular distance than 55° between the CO_2 laser spot and the cutting tool.

4.1. Experimental setup for LAM

Machining experiments were performed on Inconel 718 workpieces using a 60 hp Jones and Lampson turret lathe equipped with an NUM 1060 controller. The motor setup is capable of a maximum of 2600 RPM spindle speed. A Convergent Energy Everlase S51 1.5 kW CO_2 laser is directed vertically to the top of the workpiece surface by reflective mirrors through a 25 mm focal length lens. In order to maintain the maximum temperature below the maximum allowable temperature for the coating, a second 500 W Nd:YAG was used to heat the machined chamfer at 45° from the vertical, 10–12° circumferentially ahead of the cutting tool, delivered through a 10 m long, 600 μm diameter fiber optic cable to a lens with a focal length of 200 mm.

Force data were collected during machining using a three component Kistler 9121 dynamometer and a Kistler Model 5184B1 amplifier. The data acquisition system with National Instruments LabView was used to process and record the signals. Temperature measurements were performed using an FLIR SC3000 infrared camera, linked with ThermoCAM2002 software. The camera is most sensitive to radiation measurements at wavelengths between 8 and 9 μm.

The workpieces were Inconel 718 supplied from Special Metals Corporation, the composition of which is shown in Table 3, and were 150 mm in length and 50 mm in diameter.

Approximately 50 mm was machined during each experiment using a Greenleaf WG-300 insert (SNGN 452-T1), which is an alumina-oxide ceramic insert reinforced with silicon-carbide whiskers. A carbide chip breaker was clamped on top of the insert for every test, approximately 0.8 mm away from the primary cutting edge.

Tool wear was characterized with two metrics, i.e., the average (VB) and notch depth. These quantities are measured at prescribed machining intervals on a Zeiss optical microscope. Typical tool failure for ceramic tools may be assumed by notch wear >1.0 mm, flank wear (VB_{ave}) >0.5 mm, or catastrophic failure of the tool insert. If these are the criteria, then current trends suggest that the tool will fail by notch wear.

After machining, the surface roughness was measured using a Surtronic 3+ surface profilometer with a 0.02 μm diamond stylus. Two sets of five circumferential R_a values were measured from the workpiece and averaged to provide the surface roughness measurement.

4.2. Experimental conditions

Table 4 shows the complete experimental test matrix used for the study of LAM of Inconel 718. In order to see the effect of changing feed and depth-of-cut on the machining results, it is important to keep T_{mr} constant. Test LAM_4 and test LAM_5 represent the machining cases where depth-of-cut is varied above and below the nominal value of 0.5 mm, while tests LAM_6 and LAM_7 show the effect of lower and higher feed than the nominal value of 0.05 mm/rev. Also, it is important to lower T_{mr} from the nominal value of 620 °C to see its effect on machinability at different work material strengths. To compare the LAM with conventional machining processes,

Table 3
Material composition of Inconel 718, in weight percent

Ni	Fe	Cr	Cb	Mo	Ti	Al	C	S
53.46	18.31	18.29	4.97	3.01	1.02	0.52	0.015	0.0004

Table 4
Experimental test matrix for LAM of Inconel 718

Test #	V (m/s)	f_r (mm/rev)	d (mm)	Dia (mm)	N (rpm)	Power (W) (CO_2)	$T_{mr,ave}$ (°C)
Conv1	2.2	0.05	0.76	30	1368	—	CONV
LAM1	2.2	0.05	0.76	29	1368	860	590
LAM2	2.2	0.05	0.76	29	1410	750	540
LAM3	2.2	0.05	0.76	28	1475	610	480
LAM4	2.2	0.05	**0.50**	30	1368	820	530
LAM5	2.2	0.05	**1.00**	30	1368	870	550
LAM6	2.2	**0.025**	0.76	28	1475	740	600
LAM7	2.2	**0.075**	0.76	28	1480	860	540
L8	**2.2**	0.1	0.76	50	840	—	CONV
L9	**3.0**	0.1	0.76	47	1220	—	CONV
L10	**4.0**	0.1	0.76	49	1560	—	CONV
L11	2.2	**0.1**	0.76	27	1590	900	540
L12	2.2	**0.15**	0.76	18	2330	600	540
L13	**1.0**	0.1	0.76	36	531	900	540
L14	**3.0**	0.1	0.76	24	2490	900	540
L15	**4.0**	0.1	0.76	31.5	2540	900	360
L16	2.2	0.1	0.76	45	945	900	**360**
L17	2.2	0.1	0.76	40.5	1037	900	**410**
L18	2.2	**0.05**	0.76	45	937	922	**450**

Invariant parameters
DOC = 0.76 mm
D_{laser,CO_2} = 4.5 mm [a]
CO_2-tool lead = 1.7 mm

$\alpha_{CO_2,graphite} = 0.8$
$Emiss_{CO_2,graphite} = 0.85$

$t_{preheat}$ = 2 s CO_2 and 2 s both lasers
$D_{laser,YAG}$ = 3.0 mm
YAG-tool lead = 0.7 mm
YAG-tool angle = 10–12°
YAG-vertical angle = 45°
$\alpha_{YAG} = 0.3$
$Emiss_{YAG} = 0.20$
P_{YAG} = 500 W

Bold type represents the value of the parameter varied.
[a]Varies from 4.5 to 6.5 mm.

a conventional machining condition similar to the nominal LAM case (test LAM_1) has been used and tool lives of both these processes have been compared. The invariant process parameters include the cutting speed, $v = 2.2\,\mathrm{m/s}$, laser beam diameter, $D_\mathrm{l} = 4.5\,\mathrm{mm}$, laser-tool lead, $L_\mathrm{l} = 1.7\,\mathrm{mm}$, preheat time, $t_\mathrm{p} = 4\,\mathrm{s}$, workpiece emissivity, $\varepsilon_\mathrm{pyro} = 0.85$, and absorptivity, $\alpha = 0.8$. Here, it is important to understand that laser power and RPM (constant velocity) do not affect the machining process directly but only influence T_mr and T_max. Therefore, with changing workpiece diameters, the laser power and RPM have been suitably varied such that required thermal fields are obtained.

There is no optical access to the laser spot and material removal plane during an LAM experiment; therefore, T_max and T_mr are predicted by the thermal model. Validation of the model was achieved by comparing the predicted surface temperature at the pyrometer location with the measured value during actual tests.

The three components of the cutting forces were collected at 1000 Hz, and the data between $t = 25$ and 32 s were averaged and used to compare different operating conditions. Fig. 12 shows a marked decrease in u_c with increasing T_mr. By increasing T_mr from 0 °C (conventional machining) to 620 °C, the specific cutting energy, u_c, is reduced by 25%.

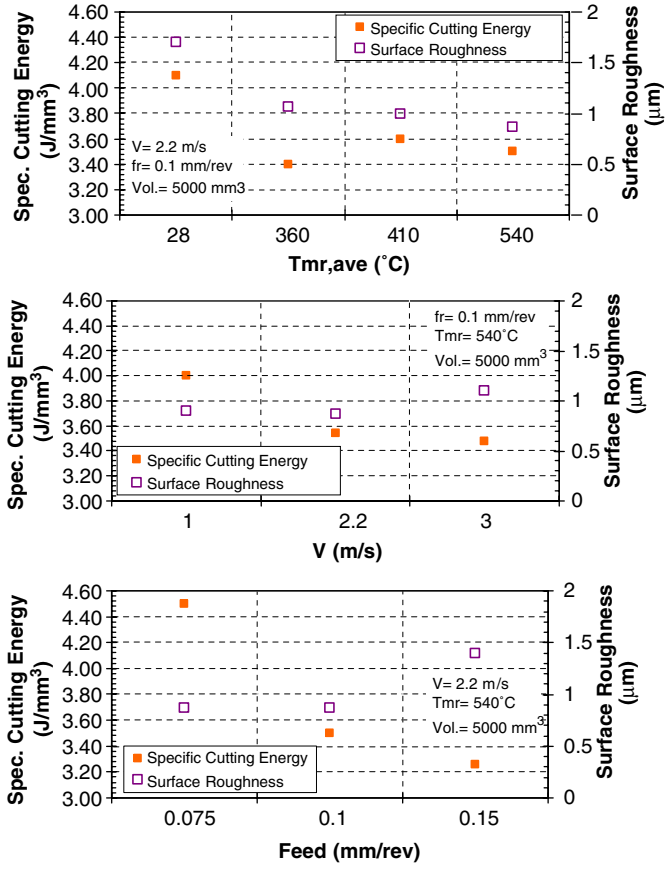

Fig. 12. Specific cutting energy and surface roughness vs. $T_\mathrm{mr,ave}$, velocity, and feed, measured after removing 5000 mm^3 of material.

4.3. Parametric testing of Inconel 718 thermal model

It is desirable that a relationship be developed to determine the average material removal temperature due to laser heating as a function of machining, laser, and workpiece parameters. A statistical analysis was performed on the predicted temperature values from the thermal model using the SAS software. The obtained equation shows the predicted correlation between laser parameters and the average material removal temperature. Although including more parameters in the analysis provided slightly better correlation, this equation incorporates only the most pertinent factors affecting T_mr to provide a good correlation and yet facilitate the use of

$$T_\mathrm{mr,ave} = 27,890\,\frac{P_{\mathrm{CO}_2}^{0.086}\,P_\mathrm{YAG}^{0.031}}{\mathrm{Dia}^{0.95}\,f^{0.32}}. \tag{3}$$

Both power terms are in W, Dia is the diameter of the workpiece in mm, and f is the feedrate in mm/min.

4.4. Machining results

4.4.1. Specific cutting energy and surface roughness

The specific cutting energy decreases with increasing material removal temperatures, cutting speed, and feed, as seen in Fig. 12. There is a large decrease in specific cutting energy between conventional machining and LAM at 360 °C, but very little change in specific cutting energy above this temperature. The specific cutting energy decreases significantly as speed is increased from 1 to 2.2 m/s, but shows only a slight decrease at cutting speeds above 2.2 m/s. Feed has a large effect on specific cutting energy and, as seen in Fig. 12, as feed increases from 0.075 mm/rev, the decrease in specific cutting energy is substantial, but the amount of decrease lessens as feed increases further.

Nickel-based superalloys will generally exhibit a significant decrease in specific cutting energy from conventional machining to "low temperature" LAM (around $T_\mathrm{mr,ave} = 300\,^\circ\mathrm{C}$), and another significant decrease in specific cutting energy will generally be observed at higher temperatures when the strength of the material is significantly reduced. In the current experiments, the initial decrease in specific cutting energy has been measured, but the second decrease in specific cutting energy is not observed, suggesting that the lowest material strength has not been achieved. Therefore, further benefits might be realized as $T_\mathrm{mr,ave}$ is increased even above 540 °C, if the tool life continues to be defined by notch wear, instead of the slowly increasing flank wear.

The surface roughness improves as material removal temperature is increased, from 1.7 µm in conventional machining to 0.9 µm during LAM at 540 °C. As cutting speed is increased to 3 m/s, the surface roughness increases marginally due to increased tearing of the material. The surface roughness does not change from 0.87 µm at feeds of

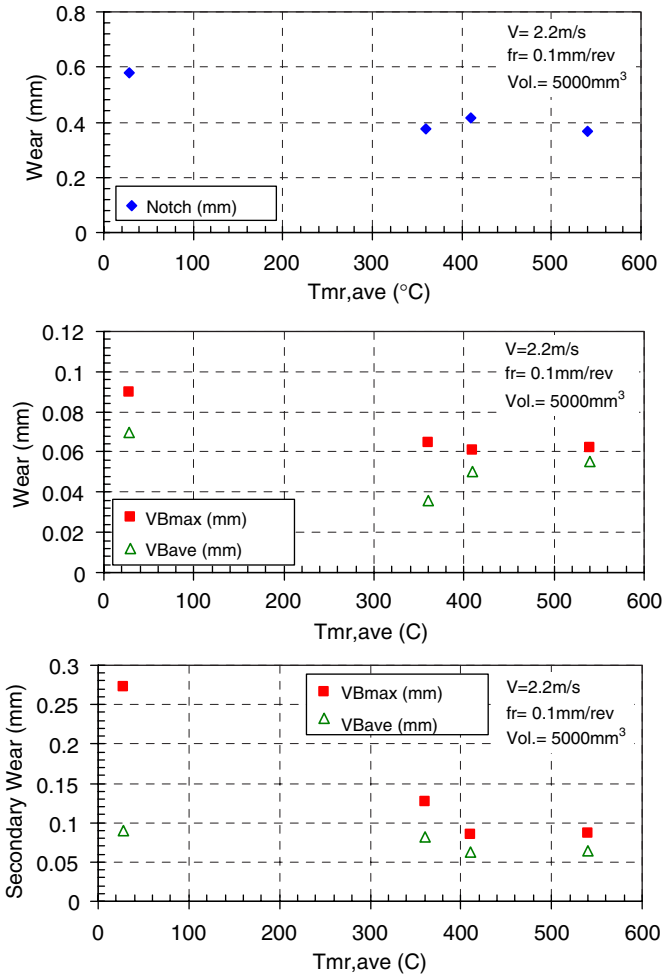

Fig. 13. (a) Notch wear, (b) primary flank wear, and (c) wear on the secondary face measured at approximately 5000 mm^3 of material removed (L8, L16, L17, L11) ($V = 2.2$ m/s, $fr = 0.1$ mm/rev, $d = 0.76$ mm).

0.075 and 0.1 mm/rev, but when the feed is increased to 0.15 mm/rev, a large increase is measured. Because of the small diameter of these workpieces, slight chatter marks were seen initially during the second cut at 0.15 mm/rev, which ultimately may have adversely affected the surface roughness. The surface roughness improves during LAM according to the facilitated material removal caused by laser heating. Also, due to the large beam diameter of the CO_2 laser, irradiation of the beam on the machined surface reduces the sharpness the surface peaks and improves surface roughness.

4.4.2. Tool wear

The effects of various machining parameters on tool wear are presented in this section.

Temperature effects: Increasing the material removal zone temperature decreases the amount of notch wear from 0.58 mm in conventional machining to 0.36 mm with LAM at 540 °C (see Fig. 13). The maximum flank wear on the primary face decreases with increasing $T_{mr,ave}$, and although the average flank wear on the primary face during LAM is lower than conventional machining, it increases as $T_{mr,ave}$ increases from 360 to 540 °C. An increase in temperature creates a smaller temperature gradient in the tool and VB_{ave} approaches VB_{max} values as the primary flank of the tool wears more uniformly. With increasing temperature, a large decrease is also seen in the maximum flank wear on the secondary face and there is a slight decrease in VB_{ave} on the secondary face. Above 400 °C, the difference between maximum and average wear on the secondary face is not affected by increasing temperatures.

Velocity effects: Increasing the velocity from 1 to 3 m/s is beneficial during LAM, in that notch wear is decreased by a half (0.63 mm compared to 0.31 mm), which is contrary to conventional machining results. Maximum and average flank wear on the primary face is also reduced (Fig. 14). The average flank wear on the secondary face is not influenced as speed is increased, but the maximum flank wear on the secondary face is significantly reduced at speeds higher than 1.0 m/s.

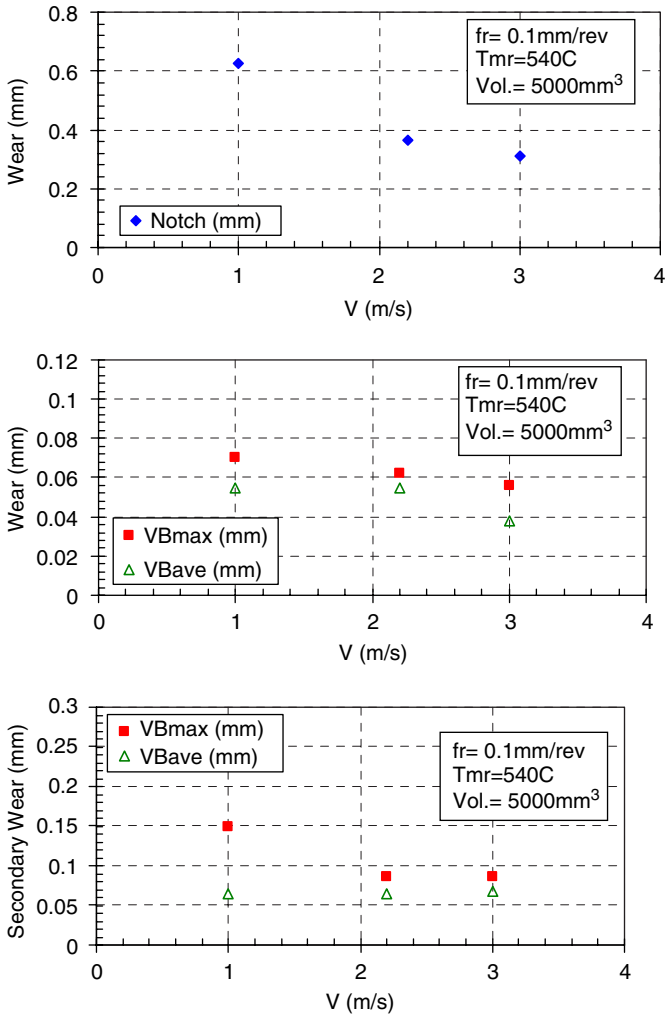

Fig. 14. (a) Notch wear, (b) primary flank wear, and (c) wear on the secondary face measured at approximately 5000 mm^3 of material removed (L13, L11, L14) ($fr = 0.1$ mm/rev, $d = 0.76$ mm, $T_{mr,ave} = 540$ °C).

Feed effects: Increasing the feed during LAM from 0.075 mm/rev decreases the notch wear, wear on the primary face, and the wear on the secondary face (Fig. 15). As feed is increased the difference between the maximum and average flank wear on the primary face decreases. Actually, any effect that increases the temperature of the cutting tool will decrease the difference between the maximum and average flank wear by creating smaller temperature gradients on the tool causing more uniform wear of the cutting tool.

4.4.3. Chip morphology and residual stresses

Chip removal plays a vital role in determining the quality of surface finish, and also in the amount of notch wear. During conventional machining, the chips are very silvery in color and form a fairly consistent curl. As speed increases during conventional machining, the tightness of the curl in the chips decreases. An increase in cutting speed increases the temperature at the tool–chip interface and reduces the friction, thus resulting in thinner chips and reduced the chip curl. During LAM, the amount of chip curvature is diminished for the same speeds as conventional machining.

The chips formed are generally categorized as "shear localized chips", which means the bulk of the chip material is not strained, but small shear bands are formed during removal of the chip as explained earlier. Due to the increased machining temperatures associated with LAM, the chips are brown, blue, or purple. The higher temperatures increase the ductility of the material, and decrease the amount of notching which occurs in the cutting tool. The jagged torn edge caused by the lateral flow of the material during removal is larger during LAM than conventional machining, but occurs more frequently during conventional machining.

The residual stresses were measured after LAM using the X-ray diffraction. Cu Kα radiation at the (420) lattice plane was utilized. The measured residual stresses are about 200–300 MPa in the hoop direction and −90 to −220 MPa in the axial direction. While it is known that turning processes usually yield tensile residual stresses, the compressive residual stresses in the axial direction indicate that LAM does not yield any adverse effect on the resultant subsurface.

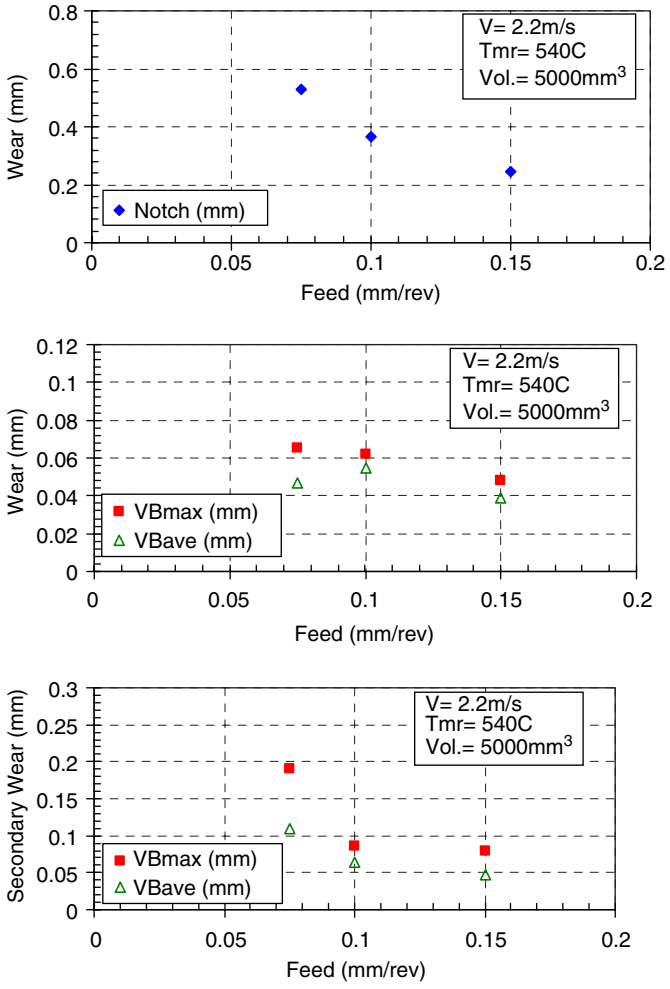

Fig. 15. (a) Notch wear, (b) primary flank wear, and (c) wear on the secondary face measured at approximately 5000 mm^3 of material removed (LAM7, L11, L12) ($V = 2.2$ m/s, $d = 0.76$ mm, $T_{mr,ave} = 540$ °C).

5. Economic analysis

Assume that one part requires the removal of 1 m axial length of material, at a constant workpiece diameter of 25 mm and depth-of-cut of 0.76 mm (total volume removed is 58,000 mm^3). The ceramic tools are considered failed when the notch wear measures over 1 mm in size, and the carbide tool is assumed failed according to the Taylor tool life equation developed in Novak [4]: $VT^{0.32} = 1.90$, where the units of V and T are given in m/s and min, respectively. This tool life equation assumes tool failure when flank wear is greater than 0.5 mm. The carbide conditions shown compare to the following machining conditions: $V = 0.5$ m/s, $fr = 0.075$ mm/rev, $d = 0.76$ mm. Assuming that changing the tool requires 4 min, a time per part comparison has been made for each ceramic insert at 2.2 and 3.0 m/s. Ceramic tools decrease the machining time by 50% over carbide inserts due to the much larger surface speeds. LAM at 2.2 m/s will decrease the total part machining time by 30%, while a time savings of 50% can be achieved at 3.0 m/s due to significantly less tool changes.

It is assumed that operating cost will be $100/h for all tests, and that use of the laser adds $30/h, accounting for wall plug efficiency of the laser and depreciation. It is also assumed that the square ceramic tool costs $31, and has a total of eight cutting edges ($3.88/edge). The carbide tool is assumed to cost $10.00, with four cutting edges ($2.50/edge). At 3.0 m/s, savings of almost 50% could be achieved by LAM at $V = 3.0$ m/s, as shown in Fig. 16.

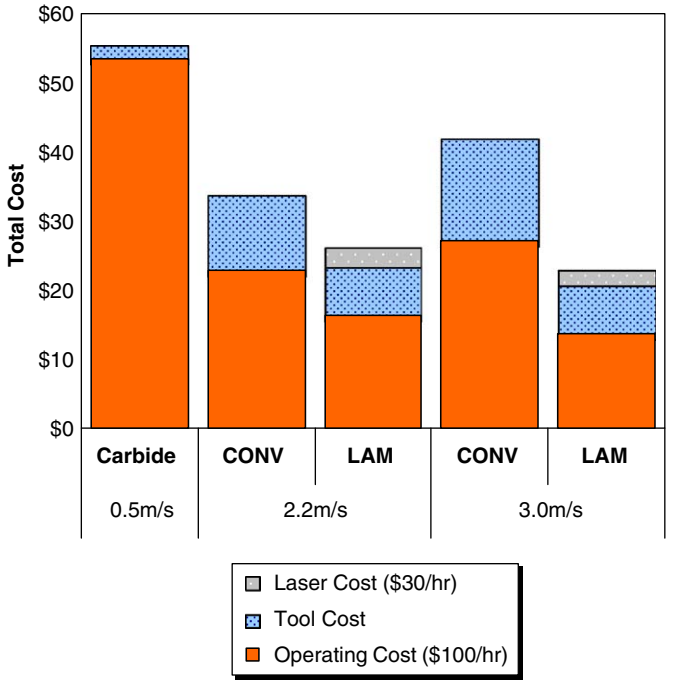

Fig. 16. Total cost comparison when machining 1 m length (or 58,000 mm^3) by conventional machining and LAM.

6. Conclusions

Laser-assisted machining (LAM) of Inconel 718 has been characterized in terms of various heating and operating conditions. Even though previous researchers have shown the feasibility of LAM of metals, inefficient laser heating techniques (absorptivity ~0.2), absence of thermal models to predict the temperature fields, poor process control without any temperature measurement, and consequently insufficient machinability benefits (surface finish, tool wear, etc.) led to absence of any further research on LAM of metals. In order to overcome these problems, governing root causes for the insufficient gain of LAM over conventional machining have been separated out and minimized. A high absorptivity of CO_2 laser energy in metals has been accomplished by choosing a suitable coating type, a right coating condition, and optimum processing parameters. This value has been evaluated to be equal to 0.80 through a systematic scientific study missing previously. The effects of speed, feed, depth-of-cut, workpiece diameter, power, and initial workpiece temperature on maximum temperature and material removal temperature have been studied. The results of LAM were experimentally analyzed by changing operating conditions, viz., feed and depth-of-cut. The surface temperatures generated during LAM were measured using the radiation pyrometer and have been shown to be well within uncertainty bound of $\pm 10\%$ of predicted temperatures.

The tool during LAM still appears to fail by notch wear, but as the average material removal temperature increases, the notch wear of the tool decreases. The average flank wear during LAM is significantly lower than conventional machining, but increases as temperature increases suggesting that a maximum beneficial temperature may be achieved before the tool rapidly fails by flank wear. The wear and chipping on the secondary face do not appear to limit tool life as temperature increases. Specific cutting energy decreases significantly during LAM from conventional machining, but shows little change at material removal temperatures between 360 and 540 °C. Surface roughness improves two-fold as temperature increases from room temperature to 540 °C. The elevated temperatures during LAM cause less pressure fluctuations at the DOC line caused by the jagged edge of the removed chip, reducing the amount of notch wear to the tool.

As velocity is increased from 1.0 to 3.0 m/s, notch wear is decreased by half, and primary flank wear also decreases. The maximum secondary wear is significantly lower at speeds above 2.2 m/s than at 1.0 m/s, although little change is seen in the secondary wear above 2.2 m/s. An increase in velocity reduces the specific cutting energy, but increases the surface roughness slightly.

As the feed increases from 0.075 to 0.15 mm/rev, all types of wear decrease. There is little change in the maximum and average flank wear on the primary face, but wear on the secondary face is significantly reduced as the feed increases over 0.075 mm/rev. Changing the feed reduces the specific cutting energy significantly, and the surface roughness is increased at feeds over 0.1 mm/rev.

There are large economic benefits to LAM, as the cost for machining 1 m length of Inconel 718 decreases 66% from conventional carbide machining and almost 50% from conventional ceramic machining at 3.0 m/s. The time to machine the same length is also decreased by similar amounts.

Acknowledgement

The authors wish to gratefully acknowledge that this research was funded by the Indiana 21st Century Research and Technology Fund and Schlumberger.

References

[1] W. Steen, Laser Material Processing, third ed., Springer, New York, 2003.
[2] J.F. Radavich, in: E.A. Loria (Ed.), Electron Metallography of Alloy 718, Superalloys 718, 625, 706 and Various Derivatives, TMS, 1997, pp. 17–26.
[3] S. Rajagopal, D.J. Plankenhorn, V.L. Hill, Machining aerospace alloys with the aid of a 15 kW laser, Journal of Applied Metalworking 2 (3) (1982) 170–184.
[4] J.W. Novak, Plasma enhanced machining of difficult to manufacture materials, M.S.M.E. Thesis, Purdue University, West Lafayette, IN, 1995.
[5] J.W. Novak, Y.C. Shin, F.P. Incropera, Assessment of plasma enhanced machining for improved machinability of Inconel 718, ASME Journal of Manufacturing Science and Engineering 119 (1997) 125–129.

[6] C.E. Leshock, J.N. Kim, Y.C. Shin, Plasma enhanced machining of Inconel 718: modeling of workpiece temperature with plasma heating and experimental results, International Journal of Machine Tools and Manufacture 41 (2001) 877–897.
[7] B.M. Jau, S.M. Copley, M. Bass, Laser assisted machining, SME Technical Paper #MR80-846, 1980, pp. 1–15.
[8] H.E. Cline, T.R. Anthony, Heat treating and melting materials with a scanning laser or electron beam, Journal of Applied Physics 48 (1977) 3895–3900.
[9] R. Komanduri, D.G. Flom, M. Lee, Highlights of DARPA advanced machining research program, American Society of Mechanical Engineers, Production Engineering Division (Publication) PED 12 (1984) 15–36.
[10] J.C. Rozzi, F.E. Pfefferkorn, F.P. Incropera, Y.C. Shin, Transient thermal response of a rotating cylindrical silicon nitride workpiece subjected to translating laser heat source: Part I—comparison of surface temperature measurements with theoretical results, Transactions of the ASME, Journal of Heat Transfer 120 (4) (1998) 899–906.
[11] J.C. Rozzi, F.E. Pfefferkorn, F.P. Incropera, Y.C. Shin, Transient, three-dimensional heat transfer model for the laser assisted machining of a silicon nitride ceramic: Part I—comparison with measured surface temperature histories, International Journal of Heat and Mass Transfer 43 (2000) 1409–1424.
[12] J.C. Rozzi, F.P. Incropera, Y.C. Shin, Transient, three-dimensional heat transfer model for the laser assisted machining of a silicon nitride ceramic: Part II—assessment of parametric effects, International Journal of Heat and Mass Transfer 43 (2000) 1425–1437.
[13] Y. Tian, Y.C. Shin, Thermal modeling for laser-assisted machining of silicon nitride ceramics with complex features, ASME Journal of Manufacturing Science and Engineering 128 (2) 2006.
[14] P. Rebro, Y.C. Shin, F.P. Incropera, Laser-assisted machining of reaction sintered mullite ceramics, Transactions of the ASME, Journal of Manufacturing Science and Engineering 124 (2002) 875–885.
[15] S.C. Catherine, M. Jeandin, D. Kechematr, J.P. Ricaud, L. Sabatier, Study of dynamic absorptivity at 10.6 μm (CO_2) and 1.06 μm (Nd–YAG) wavelengths as a function of temperature, Journal de Physique IV 7 (1991) 151–157.
[16] H.S. Carslaw, J.C. Jaeger, Conduction of Heat in Solids, Oxford Press, Oxford, 1959.
[17] Y.C. Shin, J.N. Kim, Plasma enhanced machining of Inconel 718, in: Proceedings of the Manufacturing Science and Engineering, Symposium on Advanced Machining and Finishing Processes of Ceramics, Composites and High Temperature Alloys, ASME IMECE, Atlanta, GA, 1996, pp. 243–249.